IEEE Access
Multidisciplinary | Rapid Review | Open Access Journal

Received September 1, 2021, accepted September 6, 2021, date of publication September 14, 2021,
date of current version October 1, 2021.

Digital Object Identifier 10.1109/ACCESS.2021.3112462

DC-Bus Capacitor Maximum Power Discharge Strategy for EV-PMSM Drive System With Small Safe Current

HAOLIN YANG, JIAQIANG YANG, (Senior Member, IEEE), AND XIAOJUN ZHANG
College of Electrical Engineering, Zhejiang University, Hangzhou 310027, China

Corresponding author: Jiaqiang Yang (yjq1998@163.com)

This work was supported in part by the National Natural Science Foundation of China under Grant 51777191, and in part by the Natural Science Foundation of Zhejiang Province under Grant LCZ19E070001.

ABSTRACT To prevent the passengers from electric shock, the DC-bus capacitor voltage of the high-voltage permanent magnet synchronous machine (PMSM)-based drives in electric vehicles (EVs) is required to decline to safe voltage as quickly as possible when emergency occurs. Considering that the discharge time for small safe current limit powertrain systems will be longer than required, this paper proposed a maximum power discharge strategy to accelerate the dissipating process and meanwhile avoid the voltage surge. Firstly, the PMSM discharge model as a generator is established on the basis of analyzing the discharge course. Secondly, the feasible reference current trajectory is presented by drawing the trajectories of the voltage, current, and power constraints. Then the maximum power discharge strategy is achieved by following the extreme points in the reference trajectory. Finally, simulation and experiment are conducted on a three-phase SPMSM powertrain system to validate the proposed algorithm can effectively shorten the discharge process.

INDEX TERMS Permanent magnet synchronous machine (PMSM), winding-based discharge, small safe current, maximum power.

I. INTRODUCTION

Since permanent magnet synchronous machines (PMSMs) have brilliant advantages of high efficiency, high power density, wide speed range, and compact structure, they have been widely applicated as main power source in electric vehicle (EV) powertrain systems [1]–[9]. The topology of EV-PMSM powertrain system is shown in Fig.1, in which the pivotal units of the powertrain system are exhibited. Though the storage battery packs are used for supplying and storing power, however, the voltage of the battery is generally lower than the DC-bus voltage level in EVs. Therefore, a DC/DC converter is needed to boost the low battery voltage to a higher level. A capacitor, usually thin-film capacitor on EVs, in parallel on the DC-bus can stabilize the voltage and absorb high frequency voltage surge. Necessarily, a voltage source inverter (VSI) and a controller are installed to drive the PMSM [10]–[12].

Once there is an emergency (e.g., car collision), the breaker connecting the battery and the DC/DC inverter will be triggered to cut off the power supply. Meanwhile, the controller will give orders to shut off the inverter and the gearbox will detach from the axle, leaving the PMSM rotates with no load. In this case, the energy stored on the DC-bus cannot be consumed since the inverter is shut off, and the PMSM which is working in the generate state will feedback energy to the DC-bus through uncontrolled rectifier (UR)

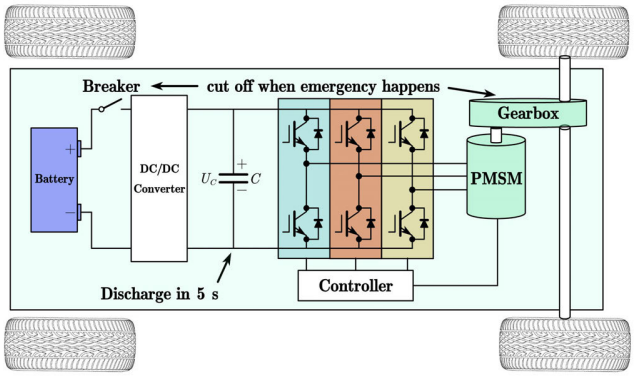

FIGURE 1. Topology of EV-PMSM powertrain system.

The associate editor coordinating the review of this manuscript and approving it for publication was Ton Duc Do.

simultaneously [13]. Nowadays, DC-bus voltage level of electric vehicles is much higher than before. For example, Tesla Model 3, BYD Tang, and Porches Taycan are 350V, 650V, and 800V respectively. Under this circumstance, if the DC- bus voltage cannot decrease to the safe level immediately, it will cause potential disastrous electric shocks, inevitably threaten the safety of both passengers and rescuers. In order to avoid such risks, United Nation Vehicle Regulation ECE R94 requires the DC-bus capacitor voltage of EVs to decrease to the safety voltage (60V) within 5 seconds [14]. To meet this requirement, several researches have been done to accelerate the dissipation of DC-bus capacitor voltage, it can be summarized to three categories: two internal methods, which are pure-winding-based method and inverter short-circuit method, and one external bleeding resistor (BR) method [15], [16].

The traditional bleeding resistor method using a switch and a resistor in parallel on the DC-bus to compose a discharge circuit, in which the power rating and maximum current rating of the bleeding resistor is supposed to be high to satisfy the required discharge time. As a result, the weight and volume of the resistor will be large, sacrificing the weight, volume, and efficiency of the EV powertrain system [17]. In terms of the inverter short-circuit method, it achieves the rapid dissipation of DC-bus voltage by switching on the MOSFET or IGBT of one or more bridge in the inverter to constitute a short circuit. Nevertheless, the essence of short-circuit strategy is to transfer the residual energy into heat on the power electronics, it will inevitably cause a high current situation in which the inverter is prone to be damaged [18]. Considering this aspect, the inverter short-circuit method is not widely adopted in industry. As for pure-winding-based discharge method, it also changes the remanent energy into the form of heat in same principle as bleeding resistor but uses PMSM windings alternatively. In [19], when a large negative d-axis current and a zero q-axis current are given, the DC-bus voltage will drop rapidly to the value equals to the back electromotive force (EMF) and track the EMF until the rotor speed is zero, in which period the remanent energy is still high, but the DC-bus voltage is low. A large negative d-axis current not only dissipates the capacitor and rotor kinetic energy immediately, but also weakens the air-gap flux and further decrease the back EMF which is tracked by DC-bus voltage. It has to be mentioned that the PMSM in [19] own the characteristic of low flux and high current limit, making it possible to pull the back EMF down to safety voltage (60 V) directly and remain sable by using the specific control strategy. For EV-PMSM powertrain system with large inertia and small safe current, the back EMF cannot be pulled down to safety voltage in most cases, even the current has reached the limit. In view of this situation, [20] concentrates no more on the stability of the DC-bus voltage but comes up with a strategy of giving a large negative d-axis current and a negative q-axis current to consume the residual energy. [20] also illustrates that since the negative q-axis current determines the speed of turning the kinetic energy into the electrical energy, excessive q-axis current will lead to the surge of DC-bus voltage, which should definitely be avoided. On this ground, a sectional q-axis current given strategy is designed under the principle of preventing DC-bus voltage surge. In spite of successfully restraining the voltage surge, this algorithm sections the reference q-axis current by 0.5s, causing the q-axis current given imprecise. Meanwhile, since the friction and capacitor energy are ignored, the discharge time is further extended.

This paper proposes a new control strategy for the EV-PMSM powertrain system with low safe current limit, discharging the DC-bus and dissipating the system energy as soon as possible without the DC-bus voltage surge. An accurate PMSM phasor diagram model as a generator is established on basis of analyzing the different stages of the discharge process. Based on this model, the maximum power discharge strategy gets the d-axis current given and q-axis current given by tracing the current locus under the voltage limit trajectory, the current limit trajectory, and the power limit trajectory, which have not been used in discharge process yet. Since the method considers the friction and the maximum system safe current, the powertrain system will dissipate the remanent energy in maximum discharge power, consequently, decreasing the DC-bus voltage and rotor speed in the fastest way.

The rest of the paper is written in the light of following structure: Section II analyzes the stages of the discharge process piecewise and establishes the PMSM discharge model as a generator. In Section III, the maximum power discharge (MPD) strategy is described on the basis of the trajectories of the voltage limit, the current limit, and the power limit, which are modeled according to Section II. Simulations are conducted to verify the effectiveness of the proposed algorithm. Then, the comparative experimental results of proposed discharge strategy and a negative d-axis reference current strategy are shown in Section IV. Section V makes a conclusion of the article.

II. ANALYSIS OF DISCHARGE PROCESS

In order to build the discharge model, the stages of the discharge process should be analyzed in advance. Meanwhile, an accurate PMSM phasor diagram model is established, which is crucial for it determines the authenticity of the voltage, current, and power trajectories, and further influences the effectiveness of the strategy. Referring to the strategy of giving a negative d-axis current and a negative q-axis current, a schematic diagram demonstrating the change of DC-bus voltage and rotor speed in the discharge process is given as Fig.2.

A. STAGES OF DISCHARGE PROCESS

Summarizing from Fig.2, the discharge process can be divided into three stages: (1) t_0-t_1: at the beginning of the discharge, the initial DC-bus voltage is much higher than the back EMF at the current speed, causing that the energy flows from DC-bus to the PMSM. The U_{dc} declines rapidly to the

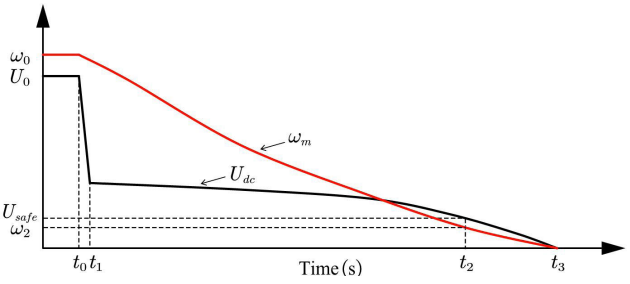

FIGURE 2. Schematic diagram of discharge process.

balanced position at t_1 in turn. The PMSM phasor diagram cannot be drawn at this stage due to the uncontrolled state of the system caused by the high voltage difference between the PMSM and DC-bus. (2) t_1-t_2: after a quick drop of the DC-bus voltage, the PMSM starts to work as a generator, where the U_{dc} is related to the rectified PMSM line voltage determined by rotor speed, flux, and current. The voltage at t_2 can be pulled down to safety voltage (60 V) in [19] because the high system safe current (150 A) weakens the flux which is originally not high, thus dramatically reducing the back EMF even though the speed is high. Notably, not only it cannot be achieved in the small safe current systems, but also the U_{dc} will surge if a large q-axis current is given. (3) t_2-t_3: With the dissipating of the rotor kinetic energy, the rotor speed decelerates from ω_0 to ω_2, at which U_{dc} rectified by the back EMF is equal to the safety voltage and will goes down continuously to 0 (t_3). For the sake of shortening the second stage, specifically, shortening the time from t_0 and t_2 to less than 5 seconds, a maximum power discharge strategy needs to be designed.

B. MODELING OF PMSM WORKING AS A GENERATOR

When operating as a generator, the PMSM is working at a fixed speed with three phases connected to the grid directly or through an uncontrolled rectifier indirectly most [21]. As for discharge process, the inverter is working as a rectifier while the speed is changing. U_{dc} is determined by the back EMF and the load, which is of great difference with the regular generator state. For the sake of drawing the voltage limit trajectory as accurate as possible, thereby getting the precise d-axis current and q-axis current in the control algorithm, an accurate PMSM phasor diagram model is established.

Focusing on the steady-state of the discharge process, the voltage equations of the PMSM can be expressed as:

$$U_d = R_s I_d - \omega_e L_q I_q \tag{1}$$

$$U_q = R_s I_q + \omega_e L_d I_d + \omega_e \phi_f \tag{2}$$

where L_d and L_q are the d axis and q axis inductances, as for surface permanent magnet synchronous machines (SPMSM), $L_d = L_q$. Moreover, ϕ_f is the permanent magnet flux linkage and ω_e is the electrical angular velocity, the relations between rotate speed n, mechanical angular velocity ω_m and ω_e is:

$$\omega_e = p\omega_m = p\frac{n \cdot 2\pi}{60} \tag{3}$$

where p is the number of pole pairs. Ignoring the mutual inductance, the phasor diagram of an IPMSM during the discharge process, in which the load is close to be capacitive, can be depicted in Fig.3, where U and I are the phase voltage and current respectively; X is the motor inductance and for SPMSM X equals to X_d; R_s is the phase resistance. The mainly difference between motor state and generator state is whether the value of the composited I_q is positive or negative under the same reference direction. We can obtain from the phasor diagram:

$$\begin{aligned}\varphi &= \alpha + \beta \\ &= arctan(\frac{I_q}{I_d}) + arctan(\frac{IX_s}{IR_s}) \\ &= arctan(\frac{I_q}{I_d}) + arctan(\frac{\omega_e L_s}{R_s})\end{aligned} \tag{4}$$

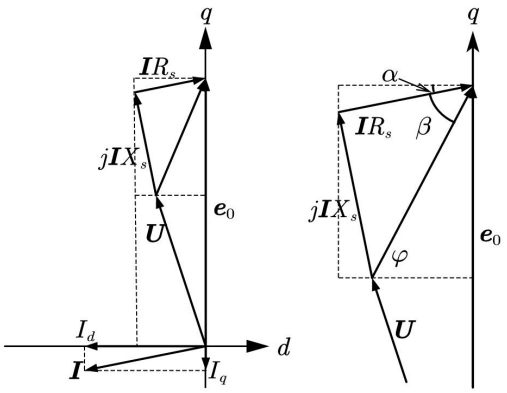

FIGURE 3. The phasor diagram of PMSM during discharge process.

Thus, the back EMF e_0 satisfies the equation:

$$e_0 = \sqrt{U^2 - (U_z cos\varphi)^2} + U_Z sin\varphi \tag{5}$$

$$U_Z = I\sqrt{R_s^2 + (\omega_e L_s)^2} \tag{6}$$

where I is the numeric value of the phase current. For a PMSM, the back EMF is related to the rotor speed and flux linkage, which can be expressed as:

$$e_0 = K_e \psi_f n = \omega_e \psi_f \tag{7}$$

where K_e is the back EMF constant which is determined mainly by the number of pole pairs. A discharge simulation with parameters in Table 1 has been done to verify the above expression of e_0, results are demonstrated in Fig.4. In order to set up the DC-bus voltage, the traditional discharge strategy is executed at 0.01 second with an initial angular

TABLE 1. Powertrain system parameters.

Symbol	Quantity	Value
Ψ_f	permanent magnetic flux linkage	0.12Wb
L_d	d-axis inductance	1.1mH
L_q	q-axis inductance	1.1mH
p	number of pole pairs	4
R_S	stator winding resistance	0.307Ω
J	moment of inertia	0.3 kg·m^2
V_{DC}	DC-bus voltage	310V
I_{max}	system safe current	30A
C	DC-bus capacitor	420μF

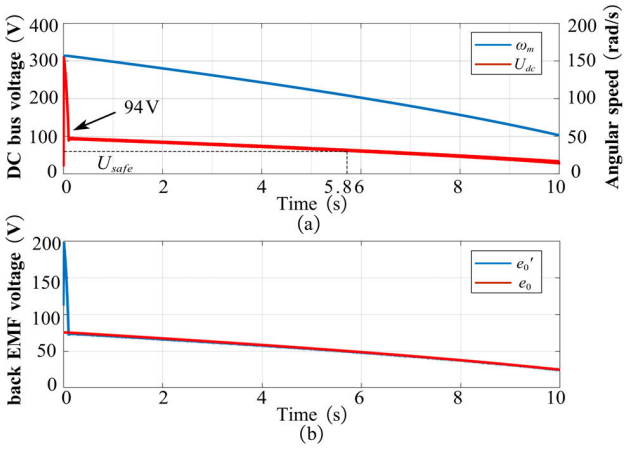

FIGURE 4. Characteristics of a typical winding-based discharge strategy with a −30A d-axis reference current and zero q-axis reference current. (a) DC-bus voltage and angular speed characteristics. (b)practical back EMF and calculated back EMF characteristics.

speed of 157 rad/s, zero q-axis current, and a reference d-axis current of −30A.

The results of the DC-bus voltage and the angular speed in Fig.4(a) coincide with the analyzed three stages during the discharge process, where the voltage drops down to 140V at the beginning of the discharge instead of directly down to the safety voltage because of the small safe current limit. After 5.8s, U_{dc} drops to the safety voltage. In Fig.4(b), e_0' is the calculated back EMF based on (4), (5), and (6) while e_0 is the actual back EMF obtained from (7). As the consequences illustrate in Fig.4(b), the back EMF e_0' which is calculated after a phasor synthesis meets the result of practical back EMF e_0 basically, except for the first stage of discharge process where the U_{dc} is much higher than the back EMF, which cannot be equal to the calculated value theoretically. Though the first stage of the discharge is uncontrollable, the DC-bus voltage will meet (5) rapidly and follow it for the rest of the discharging time, making it possible to get the expression of the U_{dc}, which is essential for the voltage limit trajectory and the control algorithm. After a transformation of (5), the DC-bus voltage can be written as (8). Based on the proposed generator model of the PMSM during discharge, the locus of the current as the core of the strategy, will be analyzed in Section III.

$$\begin{cases} U_{dc} = \sqrt{3} \cdot \sqrt{\left(\omega_e \psi_f\right)^2 - 2ab\omega_e\psi_f + b^2} \\ a = sin\left(arctg(\dfrac{I_q}{I_d}) + arctg(\dfrac{\omega_e L_s}{R_s})\right) \\ b = I\sqrt{R_s^2 + (\omega_e L_s)^2} \end{cases} \tag{8}$$

III. MAXIMUM POWER DISCHARGE STRATEGY BASED ON THE CURRENT TRAJECTOR

Since the winding-based discharge strategy uses motor resistance to dissipate the extra energy, the discharge power mainly depends on the current in the motor. Meanwhile, the transferred power from kinetic to electrical energy is determined by the electromagnetic power (q-axis current). A large electromagnetic power beyond the dissipating power, which is limited by the maximum permitted current, will cause the DC-bus voltage surge. At the same time, the voltage equation (1) and (2) needs to satisfy the declining DC-bus voltage. Thus, an optimal d-axis current and q-axis current given strategy is proposed on the basis of the trajectories of the voltage limit, the current limit, and the power limit.

A. MULTIPLE LIMITS OF THE CURRENT TRAJECTORY

Except for the (1), (2), and (8) at the generator state, the transferred power of the PMSM is:

$$P_{trans} = -\frac{3}{2} p \psi_f I_q \omega_m \tag{9}$$

The dissipating power of the motor consists two parts: stator copper losses and iron losses, and they can be written as:

$$P_{dis} = \underbrace{\frac{3}{2}\left(I_d^2 + I_q^2\right) R_s}_{P_{Cu}} + \underbrace{\frac{3}{2}\frac{U_d^2 + U_q^2}{R_c}}_{P_{Fe}} \tag{10}$$

1) CURRENT LIMIT

The current limit is decided by the minimum permitted value between the inverter and the motor, which can be specified as:

$$I_{max} = min\left\{I_{max\_inverter}, I_{max\_motor}\right\} \tag{11}$$

In d-q plane, the current limit is:

$$I_d^2 + I_q^2 \le I_{max}^2 \tag{12}$$

$$I_d \ge -\frac{\psi_f}{L_d} \tag{13}$$

where (12) can be drawn as the current limit circle in Fig.5 and (13) is the critical d-axis current in case of demagnetization.

2) VOLTAGE LIMIT

The maximum DC-bus voltage utilization for space vector pulse width modulation (SVPWM) modulation is $\sqrt{3}$, as a

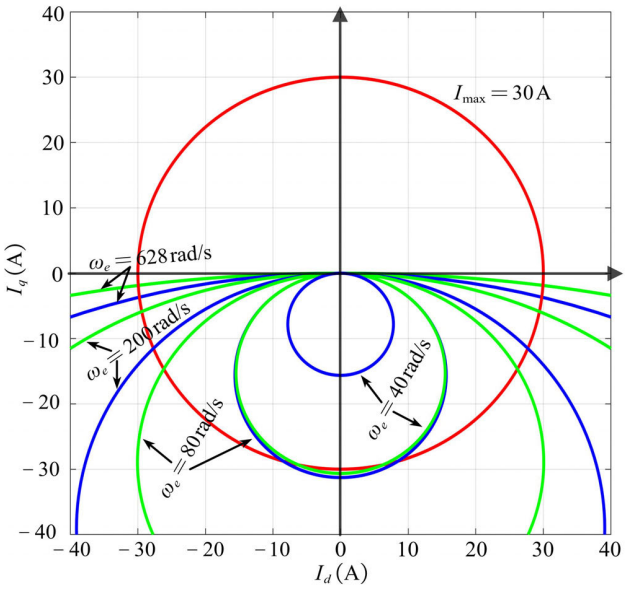

FIGURE 5. Simulation of current limit (red line), voltage limit (green line), and power limit (blue line) trajectories for SPMSM in Table 1 from 1500r/min (ω_e = 628rad/s) to 0.

result, the voltage limit in d-q plane can be defined as:

$$U_d^2 + U_q^2 \le \left(\frac{U_{dc}}{\sqrt{3}}\right)^2 \tag{14}$$

Unlike the regular voltage limit in the normal strategy [22], [23], U_{dc} is continuously declining during the discharge period. Substituting (1), (2), and (8) into (14), the voltage limit can be written as:

$$\begin{aligned}&\left(R_s^2 + \omega_e^2 L_d^2\right) I_d^2 + 2\omega_e^2 L_d \psi_f I_d + \left(R_s^2 + \omega_e^2 L_q^2\right) I_q^2 \\ &\quad + 2R_s \omega_e \psi_f I_q + 2R_s \omega_e \left(L_d - L_q\right) I_d I_q + \omega_e^2 \psi_f^2 \\ &\le \omega_e^2 \psi_f^2 - 2ab\omega_e \psi_f + b^2\end{aligned} \tag{15}$$

For SPMSM ($L_d = L_q = L_s$), ignoring the iron losses and the stator resistance voltage, the trajectory of (14) in d-q plane turns to be an ellipse:

$$\frac{I_d^2}{\frac{\omega_e^2 \psi_f^2}{R_s^2 + \omega_e^2 L_s^2}} + \frac{\left(I_q + \frac{R_s \omega_e \psi_f}{R_s^2 + \omega_e^2 L_s^2}\right)}{\frac{R_s^2 \omega_e^2 \psi_f^2}{\left(R_s^2 + \omega_e^2 L_s^2\right)^2}} = 1 \tag{16}$$

As seen in Fig.5, the center of the ellipse is on the negative shaft of the q-axis and will move away from the origin when $\omega_e \le R_s/L_s$, and then move towards zero as speed increases.

3) POWER LIMIT

For the sake of avoiding DC-bus voltage surge, the transfer power must obey the principle $P_{conv} \le P_{dis}$:

$$-\frac{3}{2} p \psi_f I_q \omega_m \le \frac{3}{2}\left(I_d^2 + I_q^2\right) R_s + \frac{3}{2}\frac{U_d^2 + U_q^2}{R_c} \tag{17}$$

According to (1) and (2), (17) can be specifically written as:

$$\begin{aligned}&\left(I_d + \frac{\omega_e^2 L_s \psi_f}{R_s^2 + R_c R_s + \omega_e^2 L_s^2}\right)^2 + \left(I_q + \frac{\left(R_s + 0.5R_c\right)\omega_e \psi_f}{R_s^2 + R_c R_s + \omega_e^2 L_s^2}\right)^2 \\ &\ge \left(\frac{0.5 R_c \omega_e \psi_f}{R_s^2 + R_c R_s + \omega_e^2 L_s^2}\right)^2\end{aligned} \tag{18}$$

Considering R_c is much larger than R_s at high rotor speed at the beginning of the discharge progress, the iron losses can be omitted and (16) can be approximated as:

$$I_d^2 + \left(I_q + \frac{\omega_e \psi_f}{2R_s}\right)^2 = \left(\frac{\omega_e \psi_f}{2R_s}\right)^2 \tag{19}$$

From Fig.5, it can also be seen that the trajectory of (16) is a circle with the center on the negative shaft of the q-axis, and the radius expands as speed increases.

B. PROPOSED MAXIMUM POWER DISCHARGE STRATEGY

In order to make sure the EV-PMSM powertrain system is working at a safe operating condition, the d-axis and q-axis currents of the PMSM ought to obey the limits above. It can be concluded from (12), (13), (16), and (18) that the limit trajectories are determined not only by the electrical angular speed, but also by the motor parameters. Hence, the border of the available d-axis and q-axis current giving area needs to be confirmed, which is a complex work, especially under three different trajectories.

First of all, the current limit trajectory which is a fixed circle in d-q plane is decided only by the system minimum current, making it the main limit condition. Both the voltage limit trajectory and power limit trajectory will shrink as speed decreases in Fig.5. As a result, there must be a critical speed separately for them to have intersection with the current limit trajectory. Combining (12) and (16), we can get the solution of the intersection point of current and voltage limit:

$$I_q = \frac{-R_s \psi_f \pm R_s \sqrt{\left(\psi_f^2 - L_s^2 I_{max}^2\right)}}{\omega_e L_s^2} \tag{20}$$

with the requirement:

$$4R_s^2 \omega_e^2 \left(\psi_f^2 - L_s^2 I_{max}^2\right) > 0 \tag{21}$$

According to (13), we can calculate that (21) is satisfied, which means the current limit and voltage limit always have intersection point. However, the trajectories in Fig.5 show that when ω_e is below a specific value, there is no intersection point. Thus, it has to be emphasized that even though the discriminant is greater than 0, the calculated I_q should be located in real number range of the voltage limit ellipse, or the solution will be imaginary numbers. From (16) we can get the range of I_q is:

$$I_q \in \left[-\frac{2R_s \omega_e \psi_f}{R_s^2 + \omega_e^2 L_s^2}, 0\right] \tag{22}$$

Further if the voltage limit has an intersection with the current limit, I_q must satisfy the condition:

$$I_q = \frac{-R_s\psi_f + R_s\sqrt{\left(\psi_f^2 - L_s^2 I_{max}^2\right)}}{\omega_e L_s^2} \geq -\frac{2R_s\omega_e\psi_f}{R_s^2 + \omega_e^2 L_s^2} \tag{23}$$

where the critical speed is:

$$\omega_e \geq \frac{R_s\psi_f - R_s\sqrt{\left(\psi_f^2 - L_s^2 I_{max}^2\right)}}{I_{max} L_s^2} = \omega_{th\_voltage} \tag{24}$$

Similarly, by combining (12) and (19), the solution of the intersection point of current and power limit trajectories can be calculated as:

$$I_q = \frac{-R_s I_{max}^2}{\omega_e\psi_f} \tag{25}$$

If I_q is located in the power limit circle, ω_e should satisfy the condition:

$$I_q = \frac{-R_s I_{max}^2}{\omega_e\psi_f} \geq \frac{-\omega_e\psi_f}{R_s} \tag{26}$$

$$\omega_e \geq \frac{R_s I_{max}}{\psi_f} = \omega_{th\_power} \tag{27}$$

When ω_e is large enough, both the voltage and power limit trajectory will have intersection points with current limit trajectory. Since the reference d-axis current and reference q-axis current are negative, we only concentrate on the third quadrant of the d-q plane. The value of (20) and (25) at the same speed should be compared, so as to make sure the specific area for d-axis and q-axis current to refer. The result of (20)-(25) is:

$$\frac{R_s\left(\psi_f - \sqrt{\left(\psi_f^2 - L_s^2 I_{max}^2\right)}\right)\sqrt{\left(\psi_f^2 - L_s^2 I_{max}^2\right)}}{\omega_e\psi_f L_s^2} > 0 \tag{28}$$

which means that the q-axis value of the intersection point of power limit and current limit (e.g. B in Fig.6) is smaller than that of voltage limit and current limit (e.g. A in Fig.6) all the time. On the basis of this, the available reference current area can be confirmed, for example the orange area in Fig.6 when ω_e is 200 rad/s.

As for maximum power discharge strategy, the transfer power is supposed to be as large as possible in the premise of matching the dissipating power, concretely, the q-axis current should be as small as possible in the available current area. As seen from Fig.6, when ω_e is 200 rad/s, the optimal reference current should be at B, which is the intersection point of power limit and current limit. As speed decreases, the voltage limit trajectory and the power limit trajectory will shrink towards the origin point. Both of the two trajectories have a critical speed, below which the limit will have no section with the current limit. The result of (27)-(24) is:

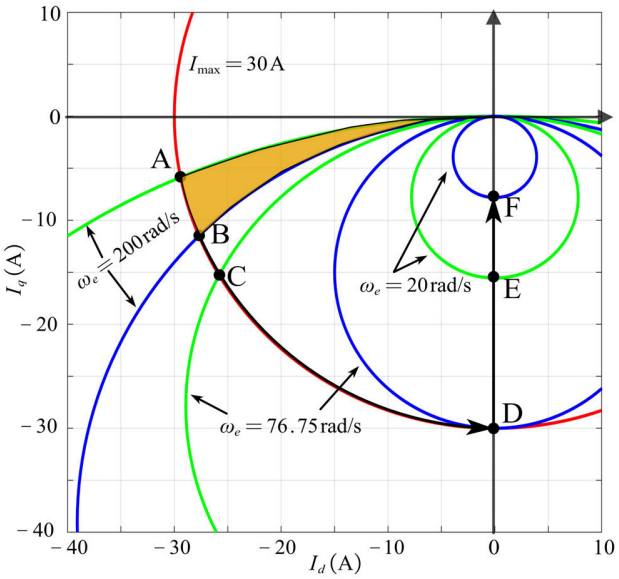

FIGURE 6. The available area and operating trajectories of *d*-axis and *q*-axis current for reference under the current limit (30A,red line), the voltage limit (green line), and the power limit (blue line).

$$\omega_{th\_power} - \omega_{th\_voltage} = \frac{R_s\left(\psi_f - \sqrt{\left(\psi_f^2 - L_s^2 I_{max}^2\right)}\right)\sqrt{\left(\psi_f^2 - L_s^2 I_{max}^2\right)}}{\psi_f I_{max} L_s^2} > 0 \tag{29}$$

which certifies that the power limit circle will detach from the current circle earlier than the voltage circle as speed decreases, causing the optimal current trajectory should follow the current limit circle until the power limit circle reach the detach point D. During this period, the optimal reference current should follow (25) at each speed. When ω_e is lower than the critical speed in (27), the power limit trajectory will detach from the current limit circle and shrink towards the origin point (from D to F). As a result, the optimal reference current cannot be at the current limit circle anymore, it is then supposed to follow the minimum q-axis value of the power limit circle to the origin point for the purpose of achieving the maximum power discharge strategy. In conclusion, the optimal current reference can be summarized as:

$$\begin{cases} I_{d\_ref} = \sqrt{I_{max}^2 - I_q^2} & \omega_e > \omega_{th} \\ I_{d\_ref} = 0 & \omega_e \leq \omega_{th} \end{cases} \tag{30}$$

$$\begin{cases} I_{q\_ref} = \dfrac{-R_s I_{max}^2}{\omega_e\psi_f} & \omega_e > \omega_{th} \\ I_{q\_ref} = -\dfrac{\omega_e\psi_f}{R_s} & \omega_e \leq \omega_{th} \end{cases} \tag{31}$$

The control block diagram of the proposed maximum power discharge strategy is shown in Fig.7, where two

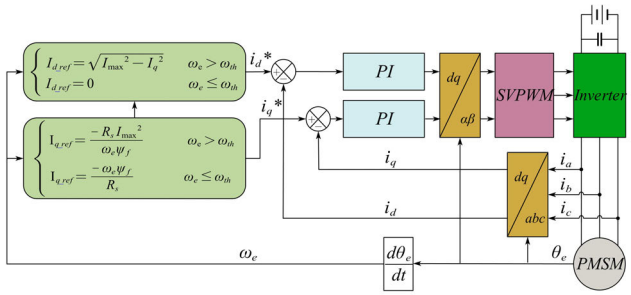

FIGURE 7. Control block diagram of the maximum discharge strategy.

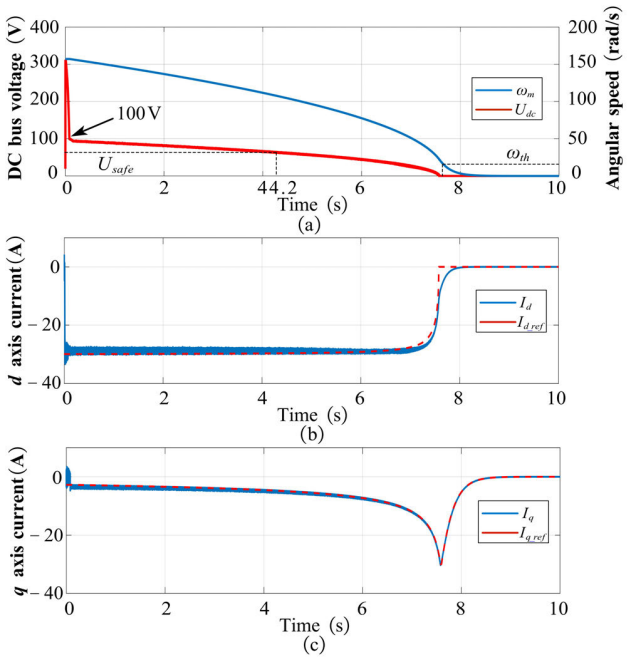

FIGURE 8. Characteristics of the proposed discharge strategy. (a) DC-bus voltage and angular speed characteristics. (b) *d*-axis current and reference. (c) *q*-axis current and reference.

PI controllers are used for current control and the SVPWM is employed as modulation in the topology.

Based on the parameters in Table 1, the simulation of the proposed strategy has been done with the results in Fig.8. Compared with the method of giving a −30A reference *d*-axis current in section II, the DC-bus voltage in this method declines to 60V within 4.2s (1.6s faster than 5.8 s in the previous method), which meets the requirement of discharge. The DC-bus voltage drops to 100V quickly in Fig.8(a) rather than 94V in Fig.4(a) mainly because the *q*-axis current in the maximum power discharge strategy is larger than that in the traditional method. Accordingly, the *d*-axis current is smaller, further affecting the back EMF.

As can be seen in Fig.8(c), the *q*-axis current follows the reference values well and can be separated into two stages. At the first stage the *q*-axis current is increasing as the speed decreases, while the *d*-axis current has no evident changes at the beginning of this stage due to the *q*-axis current is quite small. Then after the *q*-axis current almost reaches the current limit, at which the *d*-axis is almost zero and the *q*-axis current follows the reference to zero. The two stages correspond well to the trajectory A-D and D-F in Fig.6 separately and there is no voltage surge during the whole discharge process, which is also the purpose of the proposed strategy. It is worth noticing that since the *q*-axis current can be as large as the limit current after the DV-bus voltage is below 60V, the discharge time from 60V to 0V will also be much shorter than the traditional strategy, making the discharge process safer. Apparently, the simulation proves the effectiveness of the proposed method partly, the characteristics are further verified by experiments in the Section IV.

IV. EXPERIMENTAL RESULTS

The experimental platform is shown in Fig.9, with the parameters of the three-phase PMSM listed in Table 1. Three IGBT drive modules, Concept 2SD315AN, make up the inverter which is powered at 310V by a DC bus supply. A 420μF thin-film capacitor, UP3-21347K, is connected in parallel with the DC bus. The control board uses DSP TMS320F28335 as the main control chip, working at the frequency of 10kHz. Three current sample channels using LT58-S7SP8 and a voltage sample channel using LV25-P are connected to the control board for three-phase current and DC-bus voltage sampling. For the sake of simulating the real situation of powertrain system, an inertia wheel is mounted on the motor shaft. A breaker is connected in series with the dc bus to cut down the power supply when changing the algorithm. The experiment firstly uses a double closed-loop control algorithm [24] to accelerate the motor to rated speed. Once a discharge signal is given, the discharge algorithm will substitute the original algorithm while the breaker will cut off the power.

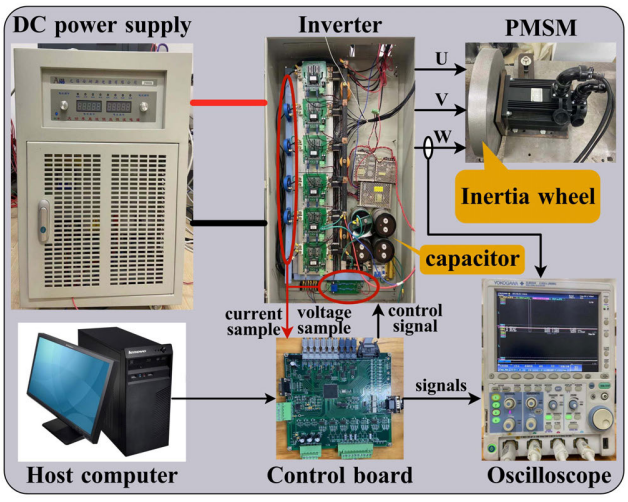

FIGURE 9. The experimental platform.

The experimental results of the traditional discharge method are demonstrated in Fig.10. The discharge is requested when the rotor speed reaches 157rad/s at around 1s,

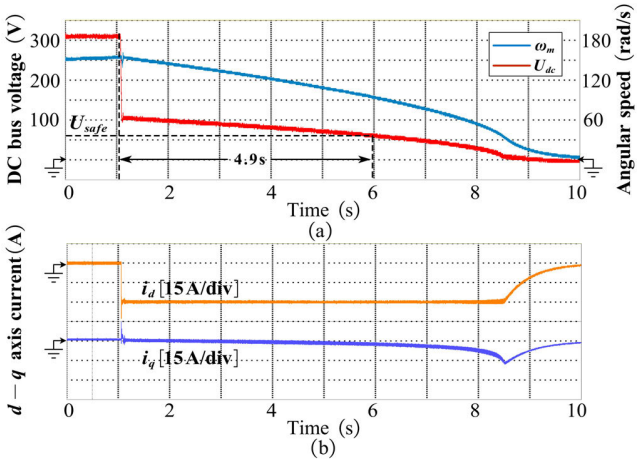

FIGURE 10. Experimental results of the traditional discharge method with a −30A *d*-axis reference current and zero *q*-axis reference current. (a) DC-bus voltage and angular speed. (b) *d*-axis and *q*-axis current.

at which time the DC-bus voltage drops to 100 V rapidly and takes 4.9 s to decline below the safety voltage, being a little bit shorter than the simulation. Once the discharge is required, the d-axis current drops to −30 A quickly and track the reference current until 8.5 s. The q-axis current is almost zero at the beginning of the discharge but gradually increasing until 8.5 s due to the cross-coupling [25], [26] effect. Then both the d-axis and q-axis current decline to zero as the energy in the motor has been almost dissipated.

Fig.10 illustrates the experimental results of the proposed discharge algorithm, which is requested at 2 s under the same speed with the traditional method. Apparently, the time for the capacitor voltage to drop to 60 V is 3.7 s (1.2 s shorter than the traditional strategy), proving that the proposed strategy can accelerate the consuming process effectively. Since the proposed algorithm obey the principle $P_{conv} \leq P_{dis}$, there is no voltage surge during the whole experiment. It can be seen from Fig.11(b) that the q-axis current is not zero at the beginning but also not too large, that is because the initial speed is high, causing the conversion power beyond the dissipating power easily even if the q-axis current is not large. As speed decreases, q-axis current will increase to the limit current while d-axis current will decrease to zero at 8.3 s, which is in accordance with the simulation. Fig.11(c) shows the characteristics of the phase A current from 4.05s to 4.1s, the current is quite sinusoidal.

In order to verify the proposed algorithm follows the maximum power trajectory, a reference current which is 1.1 times larger than in Fig.11 is given at the beginning of the experiment, the results are depicted in Fig.12. Considering that if a 1.1 times reference current is continuously giving, the DC-bus voltage will increase until it reaches the limit safe voltage of the system, the larger reference current is given for 1 s and then return to the normal value. In Fig.12(a) the DC-bus voltage surge (about 260 V) appears when the reference current is larger than the proposed value, and the time

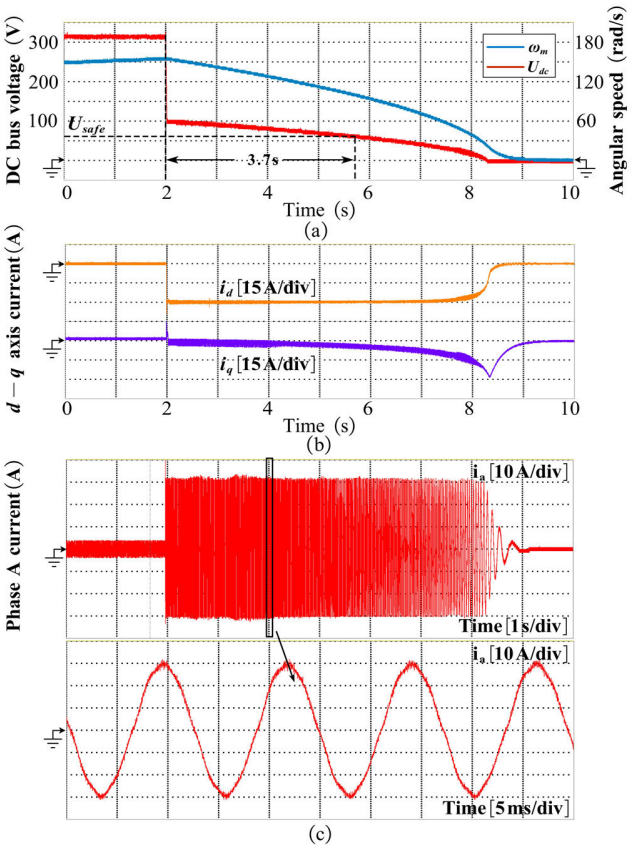

FIGURE 11. Experimental results of the proposed discharge strategy with an initial speed of 157rad/s. (a) DC-bus voltage and angular speed. (b) *d*-axis and *q*-axis current. (c)Phase A current.

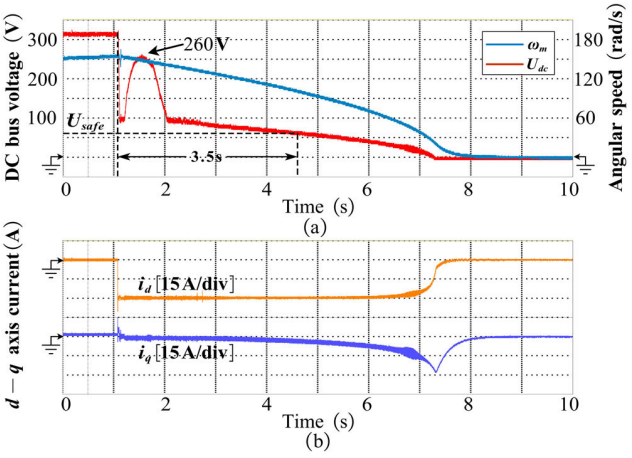

FIGURE 12. Experimental results of the proposed discharge strategy with 1.1 times reference current and an initial speed of 157 rad/s. (a) DC-bus voltage and angular speed. (b) *d*-axis and *q*-axis current.

for the voltage to decline to 60 V is 0.2 s shorter (about 3.7 s) than the proposed strategy. The experiment results prove the proposed algorithm can avoid voltage surge availably and discharge as quickly as possible at the same time.

For the sake of testifying the proposed method is suitable for all speed range, an experiment with an initial speed of 105 rad/s is carried out and the results are shown in Fig.13.

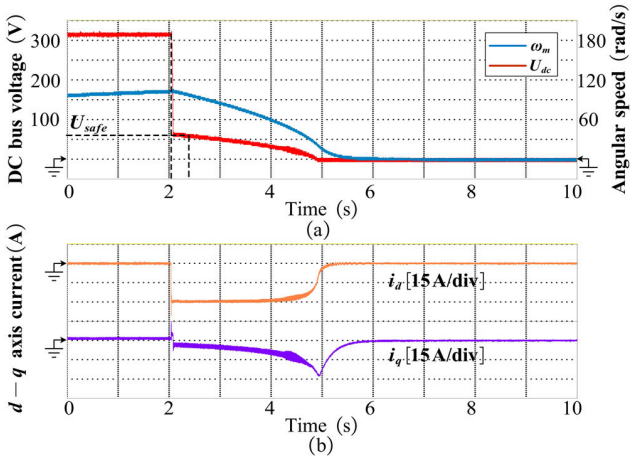

FIGURE 13. Experimental results of the proposed discharge strategy with an initial speed of 105 rad/s. (a) DC-bus voltage and angular speed. (b) d-axis and q-axis current.

Because of the low speed, the back EMF is smaller, causing the voltage drops to 60 V in only 1 s. Meanwhile, the q-axis reference current can be larger from the start due to the low initial speed. Similarly, no voltage surge appears during the discharge process.

Comparing the DC-bus voltage discharge time from 310 V to 60 V in Fig.10, Fig.11, and Fig.12, it can be concluded that the proposed method can shorten the discharge time evidently by 24.5%. Even though a larger reference current in Fig.12 can further shorten the dissipate time, the voltage surge cannot be avoided. Hence, the proposed strategy is more suitable for the EV-PMSM powertrain system to dissipate the capacitor voltage. Secondly, in order to make sure the powertrain system is working under a safe condition, three constraints of the discharge course were given by utilizing the established model. The parameters of the PMSM will barely change during the discharge process due to the short discharging time [27]. For some situations such as discharge after long time working, adding an observer for ψ_f and R_s before the discharge algorithm is switched on will improve the accuracy of the algorithm.

V. CONCLUSION

This paper proposes a novel maximum power discharge strategy based on the internal windings to meet the discharge requirement as quickly as possible without voltage surge for EV-PMSM powertrain system. The contributions and novelties of this paper are as follows:

1) An accurate PMSM phasor diagram model as a generator is established on basis of analyzing the different stages of the discharge process. Simulations are conducted to verify the accuracy of the established model.
2) To make sure that the powertrain system is working under a safe condition, three constraints of the discharge course were given by utilizing the established model. By drawing the trajectories of the current limit, voltage limit, and power limit, an algorithm of finding the optimal reference d-axis and q-axis current is proposed. This algorithm achieves the maximum power discharge without voltage surge for large inertia and small safe current system.

The simulations and experiments were carried out on a PMSM powertrain platform, proving that the proposed strategy can shorten the discharging time effectively compared with the traditional method, and the voltage surge can be avoided at the same time. Overall, the proposed discharging method can improve not only the safety level of the EV-PMSM powertrain system when accident occurs, but also the applicability of the powertrain system with different parameters such as safe current and inertia.

REFERENCES

[1] J. Wu, J. Wang, C. Gan, Q. Sun, and W. Kong, "Efficiency optimization of PMSM drives using field-circuit coupled FEM for EV/HEV applications," *IEEE Access*, vol. 6, pp. 15192–15201, 2018.
[2] G. Wang, L. Yang, G. Zhang, X. Zhang, and D. Xu, "Comparative investigation of pseudorandom high-frequency signal injection schemes for sensorless IPMSM drives," *IEEE Trans. Power Electron.*, vol. 32, no. 3, pp. 2123–2132, Mar. 2017.
[3] J. Lara, J. Xu, and A. Chandra, "Effects of rotor position error in the performance of field-oriented-controlled PMSM drives for electric vehicle traction applications," *IEEE Trans. Ind. Electron.*, vol. 63, no. 8, pp. 4738–4751, Aug. 2016.
[4] L. Chu, F. Zhou, J. Guo, and L. Yao, "Research of flux-weakening control strategy for PMSM used in electric vehicle based on stator current compensation," in *Proc. Int. Conf. Transp., Mech., Electr. Eng. (TMEE)*, Dec. 2011, pp. 1601–1604.
[5] C. Gong, Y. Hu, J. Gao, Y. Wang, and L. Yan, "An improved delay-suppressed sliding-mode observer for sensorless vector-controlled PMSM," *IEEE Trans. Ind. Electron.*, vol. 67, no. 7, pp. 5913–5923, Jul. 2020.
[6] C. Gong, Y. Hu, J. Gao, Z. Wu, J. Liu, H. Wen, and Z. Wang, "Winding-based DC-bus capacitor discharge technique selection principles based on parametric analysis for EV-PMSM drives in post-crash conditions," *IEEE Trans. Power Electron.*, vol. 36, no. 3, pp. 3551–3562, Mar. 2021.
[7] G. Feng, C. Lai, K. L. V. Iyer, and N. C. Kar, "Improved high-frequency voltage injection based permanent magnet temperature estimation for PMSM condition monitoring for EV applications," *IEEE Trans. Veh. Technol.*, vol. 67, no. 1, pp. 216–225, Jan. 2018.
[8] X. Zhang and J. Yang, "A robust flywheel energy storage system discharge strategy for wide speed range operation," *IEEE Trans. Ind. Electron.*, vol. 64, no. 10, pp. 7862–7873, Oct. 2017.
[9] C. Gong, Y. Hu, K. Ni, J. Liu, and J. Gao, "SM load torque observer-based FCS-MPDSC with single prediction horizon for high dynamics of surface-mounted PMSM," *IEEE Trans. Power Electron.*, vol. 35, no. 1, pp. 20–24, Jan. 2020.
[10] Z. Wang, T. W. Ching, S. Huang, H. Wang, and T. Xu, "Challenges faced by electric vehicle motors and their solutions," *IEEE Access*, vol. 9, pp. 5228–5249, 2021.
[11] S. Kumar, R. Sreejith, and B. Singh, "Sensorless PMSM EV drive using modified enhanced PLL based sliding mode observer," in *Proc. Int. Conf. Sustain. Energy Future Electr. Transp. (SEFET)*, Jan. 2021, pp. 1–6.
[12] S. Hu, Z. Liang, W. Zhang, and X. He, "Research on the integration of hybrid energy storage system and dual three-phase PMSM drive in EV," *IEEE Trans. Ind. Electron.*, vol. 65, no. 8, pp. 6602–6611, Aug. 2018.
[13] N. Kolli, P. Pramod, and S. Bhattacharya, "Analysis of different operating modes of PMSM during regeneration with uncontrolled rectifier," in *Proc. IEEE Transp. Electrific. Conf. Expo (ITEC)*, Jun. 2020, pp. 204–209.
[14] United Nation Economic Commission for Europe Vehicle Regulation, *Unifrom Provisions Concerning the Approval of Vehicles With Regard to the Protection of the Occupants in the Event of a Frontal Collision*, Rev. 2, Annex 11, document 94, (ECE R94), Aug. 2013.
[15] X. Sun, C. Shao, Y. Wu, D. Yang, N. Yang, and Y. Li, "Study on the brake resistor and energy consuming brake process of hybrid electric vehicle," in *Proc. Int. Conf. Electr. Syst. Aircr., Railway, Ship Propuls. Road Vehicles (ESARS)*, Mar. 2015, pp. 1–6.

[16] Y. Li, J. Zhang, C. Lv, D. Kong, and C. He, "Research of regenerative braking system for electrified buses equipped with a brake resistor," in *Proc. IEEE Vehicle Power Propuls. Conf. (VPPC)*, Oct. 2013, pp. 1–5.
[17] C. Gong, Y. Hu, W. Li, J. Gao, J. Liu, H. Wen, and J. Yang, "Hybrid DC-bus capacitor discharge strategy using internal windings and external bleeder for surface-mounted PMSM-based EV powertrains in emergency," *IEEE Trans. Ind. Electron.*, vol. 68, no. 3, pp. 1905–1915, Mar. 2021.
[18] Z. Wu, X. Su, Y. Zhu, and M. Xiao, "DC link capacitor active discharge by IGBT weak short circuit," *SAE Int. J. Adv. Current Pract. Mobility*, vol. 1, no. 3, pp. 1177–1187, Apr. 2019.
[19] Z. Ke, J. Zhang, and M. W. Degner, "DC bus capacitor discharge of permanent-magnet synchronous machine drive systems for hybrid electric vehicles," *IEEE Trans. Ind. Appl.*, vol. 53, no. 2, pp. 1399–1405, Mar. 2017.
[20] C. Gong, Y. Hu, G. Chen, H. Wen, Z. Wang, and K. Ni, "A DC-bus capacitor discharge strategy for PMSM drive system with large inertia and small system safe current in EVs," *IEEE Trans. Ind. Informat.*, vol. 15, no. 8, pp. 4709–4718, Aug. 2019.
[21] C. Gong, Y. Hu, C. Gan, G. Chen, and M. Alkahtani, "Modeling, analysis, and attenuation of uncontrolled generation for IPMSM-based electric vehicles in emergency," *IEEE Trans. Ind. Electron.*, vol. 67, no. 6, pp. 4453–4462, Jun. 2020.
[22] D. P. Marcetic and P. R. Matic, "Nonregenerative braking of permanent magnet synchronous motor," *IEEE Trans. Ind. Electron.*, vol. 67, no. 10, pp. 8186–8196, Oct. 2020.
[23] K.-Y. Cho, S.-B. Yang, C.-H. Hong, and J.-C. Kim, "An efficient braking scheme for PM synchronous motor drives," in *Proc. 6th Int. Conf. Elect. Mach. Syst.*, vol. 1, Nov. 2003, pp. 80–83.
[24] P. Pillay and R. Krishnan, "Modeling, simulation, and analysis of permanent-magnet motor drives. I. The permanent-magnet synchronous motor drive," *IEEE Trans. Ind. Appl.*, vol. 25, no. 2, pp. 265–273, Mar./Apr. 1989.
[25] Z. Li and H. Li, "MTPA control of PMSM system considering saturation and cross-coupling," in *Proc. 15th Int. Conf. Elect. Mach. Syst. (ICEMS)*, Oct. 2012, pp. 1–5.
[26] K. Lee and J.-I. Ha, "Dynamic decoupling control method for PMSM drive with cross-coupling inductances," in *Proc. IEEE Appl. Power Electron. Conf. Expo. (APEC)*, Mar. 2017, pp. 563–569.
[27] D. Liang, J. Li, and R. Qu, "Sensorless control of permanent magnet synchronous machine based on second-order sliding-mode observer with online resistance estimation," *IEEE Trans. Ind. Appl.*, vol. 53, no. 4, pp. 3672–3682, Jul./Aug. 2017.

HAOLIN YANG was born in Shandong, China, in 1996. He received the B.Sc. degree in electrical engineering from Zhejiang University, Hangzhou, China, in 2019, where he is currently pursuing the M.Sc. degree in electrical engineering with the College of Electrical Engineering.

His current research interests include permanent magnet synchronous motor (PMSM) control and drives and high-voltage SIC MOSFET drives.

JIAQIANG YANG (Senior Member, IEEE) was born in Jiangsu, China, in 1970. He received the Ph.D. degree in electrical engineering from Zhejiang University, Hangzhou, China, in 2004.

Since 2004, he has been a Lecturer, an Associate Professor, and a Professor with the College of Electrical Engineering, Zhejiang University. From 2012 to 2013, he was a Research Fellow with the College of Electrical and Computer, National University of Singapore, Singapore. His research interests include active power filters, flywheel energy storage systems, and the design and control of motor for electrical vehicle.

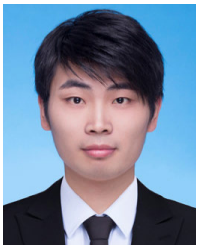

XIAOJUN ZHANG was born in Shandong, China, in 1991. He received the M.Sc. degree in electrical engineering from Zhejiang University, Hangzhou, China, in 2018, where he is currently pursuing the Ph.D. degree in electrical engineering with the Department of Electrical Engineering.

His research interests include electrical machines drives and power electronics.